Journal of
Testing and Evaluation

J. M. Marín,[1] H. Rubio,[2] J. C. García-Prada,[2] and O. Reinoso[1]

DOI: 10.1520/JTE20120345

Modeling and Simulation of 5 and 11 DOF Ball Bearing System with Localized Defect

VOL. 42 / NO. 1 / JANUARY 2014

Journal of Testing and Evaluation

doi:10.1520/JTE20120345 / Vol. 42 / No. 1 / JANUARY 2014 / available online at www.astm.org

J. M. Marín,[1] H. Rubio,[2] J. C. García-Prada,[2] and O. Reinoso[1]

Modeling and Simulation of 5 and 11 DOF Ball Bearing System with Localized Defect

Reference

Marín, J. M., Rubio, H., García-Prada, J. C., and Reinoso, O., "Modeling and Simulation of 5 and 11 DOF Ball Bearing System with Localized Defect," *Journal of Testing and Evaluation*, Vol. 42, No. 1, 2014, pp. 34–49, doi:10.1520/JTE20120345. ISSN 0090-3973.

ABSTRACT

This paper proposes a model of concentrated parameters for a rolling bearing operating in dynamic conditions with and without localized defect. The rolling bearing is modeled as a $Z+2$ df degree of freedom (DOF) system, where Z is the number of rolling elements. The radial displacement of these rolling elements is considered in this model. In the analytical formulation, the contact force between the balls and races is considered as non-linear spring-dampers, whose stiffnesses are obtained applying Hertzian elastic contact deformation theory. The equations of motion are formulated using Lagrange's equation, considering the characteristics of the individual components of a rolling bearing, such as rotor, rolling elements, and inner and outer race. The Runge-Kutta method is used to solve the non-linear differential equations of motion. The simulation is accomplished by MATLAB and SIMULINK. To validate the simulated model, we have designed a testbed to carry out. The frequency components of the signal generated by the model in simulation and the experimentally obtained signal are compared. The results achieved experimentally demonstrate the validity of the mathematical model presented here. The model provides a powerful tool to predict the satisfactory behavior of this system.

Keywords

non-linear dynamics, ball bearing, vibration, localized defect

Manuscript received December 3, 2012; accepted for publication July 8, 2013; published online October 7, 2013.

[1] Universidad Miguel Hernández de Elche Avda. Universidad s/n, CP 03202 Elche, Alicante, Spain

[2] Universidad Carlos III de Madrid Avda. Universidad No. 30, CP 28911, Leganés, Madrid, Spain

Introduction

The rolling bearing is perhaps the part of rotary machines that has the highest rate of mechanical failure (considering this rate as the number of repairs carried out on these elements over a fixed amount of time). This tendency to deteriorate is because of the fact that the bearing is the element that supports all the static and dynamic loads of the entire machine.

Various texts in the technical literature [1,2] develop, in detail, the geometric, kinematic, dynamic, and tribologic aspects of rolling bearings. However, because of the complexity of these mechanical components and the high performance standards required for them (high speeds, great load capacity, and, above all, reliability), some of these technical aspects have not been completely resolved. An analysis of the dynamic behavior of rolling bearings is decisive in the understanding of the vibratory response of rotary machines [3].

To understand all the phenomena that take place in rolling bearings, very often empirical models (derived from quasi-static processes) are employed. However, these empirical models are not too general and have large limitations [4]. With the quasi-static techniques of Harris [1] now outdated, the models currently most regarded are those that account for the dynamic effects of bearings [5].

With respect to the simulations of bearings behavior, it should be pointed out that there have been many theoretical models that have emulated the dynamics of ball bearings. Wensing [6] not only compares the 10 most efficient of these models to be found over the last 20 years, but he also calculates the damping coefficient of a rolling bearing in elasto-hydrodynamic conditions [7]. Sarangi et al. [8] propose an analytic model of a rolling bearing with elasto-hydrodynamic contact, allowing for rigidity and damping in conditions of adequate lubrication.

Among the many models of rolling bearing behavior, it is worth pointing out the analytic dynamic model developed by Walters [5] for ball bearings with a cage, which considers the slippage between the ball and raceway. This model will later be modified by Gupta [9,10] and subsequently brought up to date by the work of Tiwari et al. [11]. However, the solutions provided by the models of Walters, Gupta, and Tiwari lead to excessively long computational times.

The study of simplified systems that model the behavior of the ball and cage in rolling bearings has been carried out by numerous researchers. Yet, to date, these models have not been completely validated by laboratory results in real cases. For example, Kennel and Bupara [12] developed a simplified model to analyze the dynamic of the cage and the balls where it is assumed that the cage-balls assembly only moves on the plane of its principal diameter. Subsequently, it was shown [13] that the movements of the cage-balls assembly are too complicated to be modeled with this extreme simplification of cage movement. Fukata et al. [14] addresses the study of vibrations that derive from the non-linear dynamic response of ball bearings, which support a balanced horizontal rotor acting under constant vertical force (and allowing for the variable flexibility effect). It may be seen that resonance occurs when BPF (ball passage frequency) coincides with the system frequency and that, at certain speeds, the shaft-ball-support system may generate vibrations with sub and ultra BPF harmonics. An analytic model was then developed [15] to study and optimize the design parameters of the cage and the support rings.

In various works of Harsha et al. [16–20], analytic models are developed to predict the non-linear dynamic response of rotor-rolling bearing systems by taking into account: the balanced and horizontal rotor, the number of variable balls, the surface waviness in the outer race or inner race, the preload effect, or the cage run-out effect. To iteratively solve non-linear differential equations, Harsha uses Newmark's technique of numeric integration combined with the Newton-Raphson method. Other authors have presented analytic models of bearings similar to those of Harsha in which they have a reduced number of df and have obtained acceptable results [21].

The distribution of loads on the rolling bearings has been analyzed with models with concentrated parameters [16] and [22]. Various simulation tools have been used, often employing a dynamic simulation tools developed under the auspices of the principal bearing manufacturers, with models that use Bond Graph [23] and with models that have distributed parameters in static conditions [24]. Besides, using finite element techniques coupled with the dynamic conditions appears to open a new direction in the area of modeling of rolling bearings [25]. The subject of non-linear bearing dynamics is not completely resolved and is one that many authors continue to research [26–31].

This paper proposes an analytical model of concentrated parameters for a rolling bearing with a localized defect. The presented model is experimentally validated under different dynamic conditions and variations in the geometry of the elements of the bearing. The model takes into account the movement of the balls and the damping in the contact point leading to a complex system with $2 + Z$ DOF (where Z is the number of balls). The equations that govern the behavior of the rolling bearing are deduced by applying Lagrange's equations. Also, the settings used in the simulation are consistent with those occurring in real systems.

The remainder of the paper is structured as follows. Next, the analytical model of the bearing system is deduced. This model takes into account all the possible localized defects in its inner raceway. The section that follows presents some details about the simulation tool employed. Also in this section, simulation results for bearings with three and nine balls with and without defects are presented and discussed. Next, the testbed employed to validate the simulated model is presented. Finally, the experimental results and a comparison with the simulation results are provided.

Model Sketch

A rolling bearing dynamic model of concentrated parameters, with and without localized faults, is presented in this section. To this end, a non-linear model relates the movement of the

inner ring and the rolling elements surrounding the fixed outer ring. Although the ball bearing is the subject of this study, the model may be specified for either ball or roller bearings by adjusting the conditions of stiffness and damping, according to the situation. The rolling bearing model enables an easy variation of parameters such as spin velocity of the bearing, geometric or structural characteristics of the same, and load conditions or presence of faults. The aim of the work presented here is to validate the analytical model of a ball bearing containing localized surface defects at the inner or outer raceway.

This model will allow simulation of the behavior of the bearing vibration under different operating scenarios, with variations in the geometry of the elements of the bearing. Also, this model will allow the incorporation of different types of defects: localized defects in the inner or outer raceway, or distributed defects in the inner or outer raceway. We can find some previous works where only the rotor movement is considered and therefore the system has only two df [32]. Other works consider models with more df, but in these cases either experimental results are not provided to contrast the model or simulation settings are not appropriate (for example, the load of the bearing is lower than its required minimum load). The models have more stability issues using these values.

Equations that govern the behavior of the rolling bearing are deduced by applying Lagrange's equations. In the case of complex mechanical systems, the equations obtained using Lagrange's method are more efficient than those obtained using Newton's law. The procedure is based on Lagrange scalar magnitudes such as kinetic energy, potential energy, and virtual work. All of them can be expressed in a suitable reference system. When addressing the problem of modeling, dynamical systems based on Newton formulation of the strength, speed, accelerations, etc. will be represented with a vectorial format. However, by means of Lagrange equations, based on scalar quantities we can pay attention to these magnitudes without the necessity of employing formal vectorial methods.

To simulate the rolling bearing model, equations are implemented in MATLAB code by using the SIMULINK tool. Numerical integration is carried out by the *ode*45 method. The *ode*45 is an integration method provided by the SIMULINK Solver. This is a one-step method [33] based on the Runge-Kutta formula of the 4th and 5th order. This method gives satisfactory results for most continuum models and proves to be a good method as a first approximation when the knowledge of the system being analyzed is not sufficient. The Runge-Kutta method can be used to solve non-linear equations derived from dynamics and contacts in rotary mechanical systems [34]. The obtained results from the dynamic rolling bearing model will be studied via frequential analysis. In the process, the evolution of the spectral power of vibration of this model will be observed in relation to the variation of certain operative parameters of the rolling bearing.

Modeling of the Ball Bearing System

ROLLING BEARING SYSTEM DESCRIPTION

A real ball bearing is a mechanism with many elastic components making their analytical model very complex and with non-linear structural equations. A ball bearing system has been designed to support radial and axial load while turning at high speeds.

The rolling bearing is composed basically of an inner race joined to the axis of rotation, an outer race joined to the support of the bearing, and a set of rolling elements that can be balls or rollers with different geometries, placed between the two races. Assistant elements, cages, or tabs are employed, whose only purpose consists of keeping the rolling elements separated at certain distances between them. The cage and the rolling elements have a rotational motion around the axis of the bearing. The scheme of this rolling bearing system is shown in **Fig. 1**.

The model of the contact elements can be derived considering a mass-spring system with the corresponding damping. The outer race is fixed to the rigid surrounding, whereas the inner race is rigidly fixed to the rotor spinning at a certain angular velocity ω_{in}. Elastic deformation between the races and rolling elements, in this case balls, presents a non-linear force-deformation behavior, which is obtained by applying the Hertz theory. In the analytical model, the ball bearing is considered as a mass-spring-damping and the balls act as non-linear springs, as can be seen in **Fig. 2**.

Because Hertzian forces act only in the case of contact of the ball with the inner or the outer race, the springs act only under pressure. When the ball is separated from the rolling track, the contact force is zero. This condition makes a non-linear effect in the ball's motion equations.

FIG. 1 Rolling bearing system.

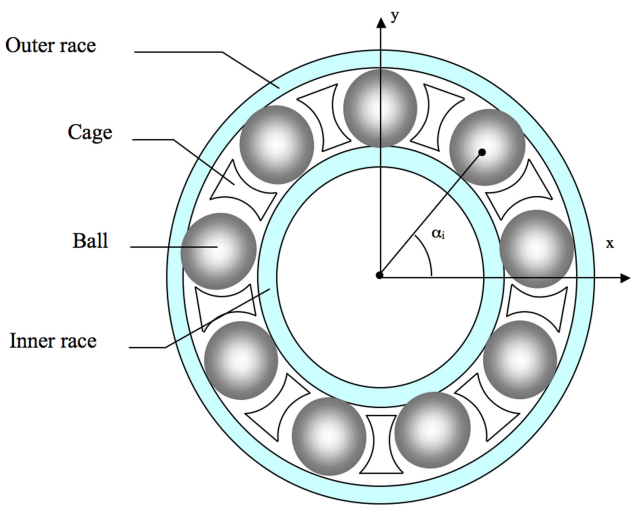

FIG. 2 Modeling the ball as non-linear spring-damper.

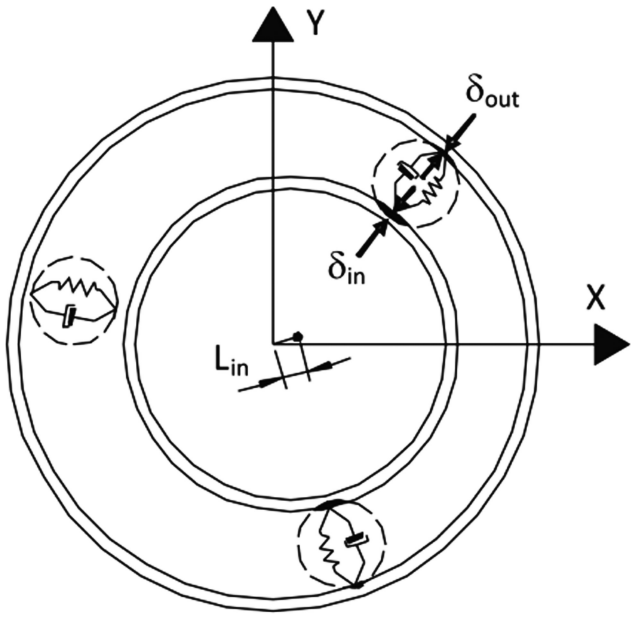

Before deriving the motion equations and to avoid an excessively complex mathematical model, we take into consideration the following assumptions [28]:

- Deformations occur according to the Hertzian theory of elasticity: small elastic motions are considered but plastic deformations are neglected.
- The balls and the rotor move in a plane. All of the elements (inner and outer races, balls, rotor, etc.) have motions only in this plane that is considered as the movement plane.
- The angular velocity of the cage is constant.
- The balls of the bearing have no angular rotation about their axes.
- All the bearing elements and the rotor are considered rigid.
- The bearing works under isothermal conditions. Therefore, dimensional variations because of temperature effects are not considered.
- We consider that there is no slipping between the balls and the surface of the races.
- The cage keeps a constant distance between the balls of the bearing. Therefore, there is no interaction between them.

DIFFERENTIAL EQUATIONS OF MOTION

In this section, we derive the equations of motion of the rolling element bearing using the Lagrange formulation. We consider a system composed by i elements with j DOF. The number of generalized coordinates (the same that the number of DOF), that allow determination of the movement, will be denoted as $q_1, q_2, q_3, \ldots, q_j$.

The displacement vector showing the location of the ith element can be denoted as:

$$r_i = f(q_1, q_2, q_3, \ldots, q_j) \tag{1}$$

The motion equations are obtained from the Lagrange equation for a set of generalized coordinates. If the system is not conservative and therefore there are dissipative forces, we can write the Lagrange equation in its most general form as [35]:

$$\frac{d}{dt}\left(\frac{\partial T}{\partial \dot{q}_j}\right) - \frac{\partial T}{\partial q_j} + \frac{\partial U}{\partial q_j} + \frac{\partial D_R}{\partial \dot{q}_j} = Q_j \tag{2}$$

where T is the kinetic energy, U is the potential energy, D_R is the Rayleigh's dissipation function, and Q_j is the nonconservative generalized force of friction. For a system with 1 degree of freedom, we have:

$$T = \frac{1}{2} m \dot{q}_1^2; \quad U = \frac{1}{2} C q_1^2; \quad D_R = \frac{1}{2} D q_1^2 \tag{3}$$

where C is the stiffness coefficient (considered by the Hooke's Law $F = C{\cdot}x$), and D is the damping coefficient.

The total kinetic and potential energy of the system can be obtained by the addition of several values of the components of the bearing. So, the total kinetic energy can be expressed as:

$$T_T = T_{\text{rotor}} + T_{\text{in}} + T_{\text{out}} + \sum_{i=1}^{Z} T_i \tag{4}$$

where T_{rotor} is the kinetic energy of the rotor, T_{in} is the kinetic energy of the inner race, T_{out} the kinetic energy of the outer race, and T_i the kinetic energy of each ball. **Table 1** represents the notation used for the rolling bearing model.

In a similar way, the total potential energy can be expressed as:

$$U_T = U_{\text{rotor}} + U_{\text{in}} + U_{\text{out}} + \sum_{i=1}^{Z} U_i + \sum_{i=1}^{Z} (U_{\text{cin}} + U_{\text{cout}}) \tag{5}$$

where U_{rotor} is the potential energy of the rotor, U_{in} is the potential energy of the inner race, U_{out} is the potential energy of the outer race, U_i is the potential energy of each ball, U_{cin} is the elastic potential energy of the contact of each ball with the inner race, and finally U_{cout} is the elastic potential energy of the contact of each ball with the outer race.

Figure 3 shows the employed notation of the generalized coordinates chosen for the model of the system. So, we have $2+3$ and $2+9$ DOF system for three and nine balls bearing, respectively. Following, the motion equations of each one of the elements that constitute the bearing are derived.

INNER RACE

The position of the mass center of the inner race with regard to the global reference system can be expressed as:

$$\overrightarrow{L_{\text{in}}} = x_{\text{in}} \vec{i} + y_{\text{in}} \vec{j} \tag{6}$$

TABLE 1 Nomenclature used in analytical model.

Item	Description	Unit
ω_{in}	Rotational speed of the inner race	rpm
r_b	Radius of each rolling element	mm
R_{in}	Radius of the inner race	mm
R_{out}	Radius of the outer race	mm
m_{in}	Mass of the inner race	kg
m_b	Mass of the rolling element	kg
m_{rotor}	Mass of the rotor	kg
L_{in}	Position of mass center of the inner race	
r_i	Radial position of the ith rolling element	
ρ_i	Position of the ith rolling element from the center of inner race	
α_i	Angular position of the ith rolling element	Degree
α_{in}	Angular position of the rotor	Degree
F_u	Unbalanced rotor force	N
F_{ex}, F_{ey}	Component of external force	N
C_{in}	Constant for Hertzian contact elastic deformation referred to ball inner raceway	$N/mm^{3/2}$
C_{out}	Constant for Hertzian contact elastic deformation referred to ball outer raceway	$N/mm^{3/2}$
D_{in}	Damping coefficient referred to ball inner raceway contact	Ns/mm
D_{out}	Damping coefficient referred to ball outer raceway contact	Ns/mm
δ_{in}	Deformation at the point of the contact of the ith ball inner raceway	mm
δ_{out}	Deformation at the point of the contact of the ith ball outer raceway	mm
h	Internal radial clearance	mm
x_{in}, y_{in}	Center of the inner race	
x_{in}^o, x_{in}^o	Initial position of the center of inner race	
r_i^o	Radial initial position of ith rolling element	mm
I_b	Moment of inertia of each rolling element	$kg.m^2$
I_{rotor}	Moment of inertia of the rotor	$kg.m^2$
I_{in}	Moment of inertia of the inner race	$kg.m^2$

The kinetic energy of the inner race can be derived as:

$$T_{in} = \frac{1}{2} m_{in} \left(\overrightarrow{\dot{L}_{in}} \cdot \overrightarrow{\dot{L}_{in}} \right) + \frac{1}{2} I_{in} \cdot \dot{\alpha}_{in}^2 \tag{7}$$

The velocity can be achieved by computing the derivative of the position of the mass center of the inner race:

FIG. 3 Mass-spring-damper model of the element.

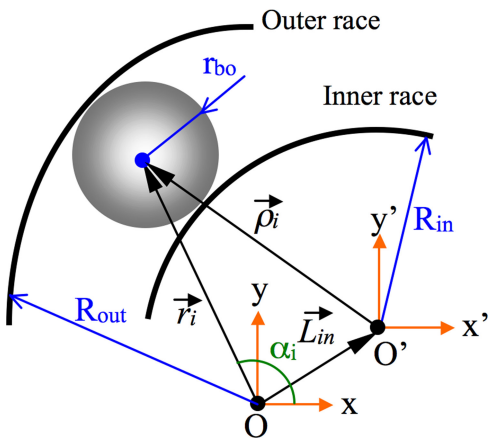

$$\overrightarrow{\dot{L}_{in}} = \dot{x}_{in} \vec{i} + \dot{y}_{in} \vec{j} \tag{8}$$

As a consequence:

$$T_{in} = \frac{1}{2} m_{in} \left(\dot{x}_{in}^2 + \dot{y}_{in}^2 \right) + \frac{1}{2} I_{in} \dot{\alpha}_{in}^2 \tag{9}$$

Taken as reference the potential energy of the mass center of the outer race, the potential energy of the inner race can be expressed as:

$$U_{in} = m_{in} g h_{in} = m_{in} g y_{in} \tag{10}$$

The components in the Lagrange equation can be achieved from the kinetic energy, potential energy, and dissipation function, computing the partial derivative with regard to the generalized coordinates $(x_{in}, y_{in}, r_1, \ldots, r_i, \ldots, r_Z)$, and computing the time derivative $(\dot{x}_{in}, \dot{y}_{in}, \dot{r}_1, \ldots, \dot{r}_i, \ldots, \dot{r}_Z)$. In this case, for the inner race we have:

$$\begin{aligned} \frac{d}{dt}\left(\frac{\partial T_{in}}{\partial \dot{x}_{in}}\right) &= \frac{d}{dt}\left(m_{in}\dot{x}_{in}\right) = m_{in}\ddot{x}_{in} \\ \frac{d}{dt}\left(\frac{\partial T_{in}}{\partial \dot{y}_{in}}\right) &= \frac{d}{dt}\left(m_{in}\dot{y}_{in}\right) = m_{in}\ddot{y}_{in} \\ \frac{\partial U_{in}}{\partial y_{in}} &= m_{in} g \end{aligned} \tag{11}$$

ROTOR

Because the rotor is joined with the inner race in the bearing, both of them have the same movement and position. Therefore, they have similar expressions for the kinetic and potential energy. Only the mass and the moment of inertia of such elements are different.

$$T_{\text{rotor}} = \frac{1}{2} m_{\text{rotor}} \left(\dot{x}_{\text{in}}^2 + \dot{y}_{\text{in}}^2\right) + \frac{1}{2} I_{\text{rotor}} \dot{\alpha}_{\text{in}}^2 \tag{12}$$

$$U_{\text{rotor}} = m_{\text{rotor}} g h_{\text{in}} = m_{\text{rotor}} g y_{\text{in}} \tag{13}$$

So, the components of the Lagrange equation for the rotor are:

$$\begin{aligned} \frac{d}{dt}\left(\frac{\partial T_{\text{rotor}}}{\partial \dot{x}_{\text{in}}}\right) &= \frac{d}{dt}\left(m_{\text{rotor}} \dot{x}_{\text{in}}\right) = m_{\text{rotor}} \ddot{x}_{\text{in}} \\ \frac{d}{dt}\left(\frac{\partial T_{\text{rotor}}}{\partial \dot{y}_{\text{in}}}\right) &= \frac{d}{dt}\left(m_{\text{rotor}}\, \dot{y}_{\text{in}}\right) = m_{\text{rotor}} \ddot{y}_{\text{in}} \\ \frac{\partial U_{\text{rotor}}}{\partial y_{\text{in}}} &= m_{\text{rotor}} g \end{aligned} \tag{14}$$

OUTER RACE

Because of the outer race fixed to a rigid surrounding, its contribution to the total kinetic and potential energy is zero.

BALLS

The position of the mass center of the ith ball i from the global reference system is:

$$\vec{r_i} = r_i \cos\alpha_i \vec{i} + r_i \sin\alpha_i \vec{j} \tag{15}$$

where α_i is the angular position of the rolling element i. The kinetic energy is:

$$T_i = \frac{1}{2} m_b \left(\vec{\dot{r}_i} \cdot \vec{\dot{r}_i}\right) + \frac{1}{2} I_b \omega_b^2 = \frac{1}{2} m_b \left(\dot{r}_i^2 + r_i^2 \dot{\alpha}_i^2\right) + \frac{1}{2} I_b \omega_b^2 \tag{16}$$

where ω_b is the angular velocity of each ball with regard to its center of mass.

We can estimate the potential energy of the rolling element i, taking as reference the center of the outer race, as:

$$U_i = m_b g h_i = m_b g r_i \sin\alpha_i \tag{17}$$

So, the components of the Lagrange equation for the ball i, are:

$$\frac{d}{dt}\left(\frac{\partial T_i}{\partial \dot{r}_i}\right) = m_b \ddot{r}_i; \quad \frac{\partial T_i}{\partial r_i} = m_b r_i \dot{\alpha}_i^2; \quad \frac{\partial U_i}{\partial r_i} = m_b g \sin\alpha_i \tag{18}$$

where $i = 1, 2, 3, \ldots, Z$ (Z being the number of balls).

CONTACT ROLLING ELEMENT-INNER RACE

The reaction force (in Newtons) as a consequence of the deformation in the contact point is:

$$F = C_{\text{in}} \delta_{\text{in}}^{\frac{3}{2}} \tag{19}$$

The work carried out can be expressed as $dW = Fd\delta$. This work is developed as an elastic potential energy:

$$\Delta W = \Delta U = \int C_{\text{in}} \delta_{\text{in}}^{\frac{3}{2}} d\delta = \frac{2}{5} C_{\text{in}} \delta_{\text{in}}^{\frac{3}{2}} \tag{20}$$

Taking into account all of the rolling elements that constitute the bearing, its elastic potential energy can be expressed as:

$$U_{\text{cin}} = \sum_{i=1}^{Z} \frac{2}{5} C_{\text{in}} \delta_{\text{in\_}i}^{\frac{5}{2}} \tag{21}$$

Considering the values of the different elements of the bearing and the position of the mass center of the ball with regard to the mass center of the inner race, ρ_i, the value of the deformation δ_{in} at the point of contact with the inner race can be expressed as:

$$\delta_{\text{in\_}i}(t) = \begin{cases} R_{\text{in}} + r_b - \rho_i & \text{if} \quad \rho_i < R_{\text{in}} + r_b \\ 0 & \text{if} \quad \rho_i \geq R_{\text{in}} + r_b \end{cases} \tag{22}$$

where ρ_i can be deduced from:

$$\rho_i = \left[r_i^2 + x_{\text{in}}^2 + y_{\text{in}}^2 - 2 r_i \cos\alpha_i x_{\text{in}} - 2 r_i \sin\alpha_i y_{\text{in}}\right]^{\frac{1}{2}} \tag{23}$$

Because only elastic potential energy exists, it is necessary to compute the variation of this energy from the generalized coordinates $(x_{\text{in}}, y_{\text{in}}, r_1, \ldots, r_i, \ldots, r_Z)$.

- Regarding to the generalized coordinate x_{in}:

$$\frac{\partial U_{\text{cin}}}{\partial x_{\text{in}}} = \frac{2}{5} C_{\text{in}} \frac{\partial}{\partial x_{\text{in}}}\left(\delta_{\text{in\_}i}^{\frac{5}{2}}\right) = -C_{\text{in}} \delta_{\text{in\_}i}^{\frac{3}{2}} \frac{x_{\text{in}} - r_i \cos\alpha_i}{\rho_i} \tag{24}$$

- Regarding the generalized coordinate y_{in}

$$\frac{\partial U_{\text{cin}}}{\partial y_{\text{in}}} = \frac{2}{5} C_{\text{in}} \frac{\partial}{\partial y_{\text{in}}}\left(\delta_{\text{in\_}i}^{\frac{5}{2}}\right) = -C_{\text{in}} \delta_{\text{in\_}i}^{\frac{3}{2}} \frac{y_{\text{in}} - r_i \sin\alpha_i}{\rho_i} \tag{25}$$

- Regarding the generalized coordinates r_1,., r_i, r_Z

$$\begin{aligned} \frac{\partial U_{\text{cin}}}{\partial r_i} &= \frac{2}{5} C_{\text{in}} \frac{\partial}{\partial r_i}\left(\delta_{\text{in\_}i}^{\frac{5}{2}}\right) \\ &= -C_{\text{in}} \delta_{\text{in\_}i}^{\frac{3}{2}} \frac{r_i - \cos\alpha_i x_{\text{in}} - \sin\alpha_i y_{\text{in}}}{\rho_i} \end{aligned} \tag{26}$$

where $i = 1, 2, 3, \ldots, Z$.

As a consequence of the contact between the ball and the race, a damping or a loss of energy can be considered, so the Rayleigh's dissipation function D_R, can be calculated as:

$$D_R = \sum_{i=1}^{Z} \frac{1}{2} D_{\text{in}} \dot{r}_i^2 \tag{27}$$

where we have considered the velocity of the ball in the global reference system. Therefore, the components of the Lagrange equation for the ball i can be expressed as $i = 1, 2, 3, \ldots, Z$:

$$\frac{\partial D_R}{\partial \dot{x}_{\text{in}}} = 0; \quad \frac{\partial D_R}{\partial \dot{y}_{\text{in}}} = 0; \quad \frac{\partial D_R}{\partial \dot{r}_i} = \sum_{i=1}^{Z} D_{\text{in}} \dot{r}_i \tag{28}$$

CONTACT ROLLING ELEMENT-OUTER RACE

The elastic potential energy from the contact rolling element and the outer race can be expressed as:

$$U_{\text{cout}} = \sum_{i=1}^{Z} \frac{2}{5} C_{\text{out}} \delta_{\text{out\_}i}^{\frac{5}{2}} \tag{29}$$

Taking into account the dimensions of the different elements of the bearing and the position of the mass center of the ball with regard to the global reference system r_i, the value of the deformation $\delta_{\text{out\_}i}$ at the point of contact at outer race is:

$$\delta_{\text{out\_}i}(t) = \begin{cases} r_i + r_b - R_{\text{out}} & \text{if} \quad r_i > R_{\text{out}} - r_b \\ 0 & \text{if} \quad r_i \leq R_{\text{out}} - r_b \end{cases}$$

Considering only potential energy, we can conclude:

- Regarding the generalized coordinate x_{in}

$$\frac{\partial U_{\text{cout}}}{\partial x_{in}} = C_{\text{out}} \delta_{\text{out\_}i}^{\frac{3}{2}} \frac{\partial \delta_{\text{out\_}i}}{\partial x_{\text{in}}} = 0 \tag{31}$$

- Regarding the generalized coordinate y_{in}

$$\frac{\partial U_{\text{cout}}}{\partial y_{in}} = C_{\text{out}} \delta_{\text{out\_}i}^{\frac{3}{2}} \frac{\partial \delta_{\text{out\_}i}}{\partial y_{\text{in}}} = 0 \tag{32}$$

- Regarding to $r_1, \ldots, r_i, \ldots, r_Z$, $(i = 1, 2, 3, \ldots, Z)$:

$$\frac{\partial U_{\text{cout}}}{\partial r_i} = C_{\text{out}} \delta_{\text{out\_}i}^{\frac{3}{2}} \frac{\partial \delta_{\text{out\_}i}}{\partial r_i} \tag{33}$$

The Rayleigh's dissipation function D_R at the point of contact at outer race is:

$$D_R = \sum_{i=1}^{Z} \frac{1}{2} D_{\text{out}} \dot{r}_i^2 \tag{34}$$

So, the components of the Lagrange equation for the rolling element i, are:

$$\frac{\partial D_R}{\partial \dot{x}_{\text{in}}} = 0; \quad \frac{\partial D_R}{\partial \dot{y}_{\text{in}}} = 0; \quad \frac{\partial D_R}{\partial \dot{r}_i} = \sum_{i=1}^{Z} D_{\text{out}} \dot{r}_i \tag{35}$$

where $i = 1, 2, 3, \ldots, Z$

MODELING OF LOCATED DEFECT

Localized defect means a single point of failure; for example, any abnormality is present in any of the items of the bearing such as cracks, pitting, chipping, etc. The simplest way to express a fault on the inner or outer race is the sudden change in the radius of curvature of the raceway. This variation can be positive or negative depending on the cause of the defect, as this may be a dimple or an impurity element interposed between the rolling element and the raceway.

In the following, the model of a localized defect in the inner race will be described. The parameters used to model the defect in the inner race are shown in **Fig. 4.** An initial position α_{di_in} is defined, the defect depth P_{d_in} and the arc length covering the defect on the inner raceway, L_{d_in} are shown in **Fig. 5.**

When the angular position of the ith ball α_i is inside the fault zone, then $\alpha_{di\_\text{in}} < \alpha_i < \alpha_{df\_\text{in}}$ as shown in **Fig. 5.**

When the ball reaches the zone of defect it has a greater freedom of movement without deformation. Obviously, when the ball is on the zone of defect a deformation will be produced depending on the load of the bearing. The radius of curvature that initially had a value R_{in} changes to R_{d_in}. This variation generates a deformation in the contact point of the ring and the ball, δ_{in}, see **Fig. 5.**

Given the above conditions, the deformation at contact points between the ith rolling element and the inner race is

$$\delta_{\text{in\_}i}(t) = \begin{cases} R_{\text{in}} + r_b - \rho_i & \text{if} \quad R_{\text{in}} + r_b > \rho_i \quad \text{and} \quad \alpha_{di\_\text{in}} \leq \alpha \leq \alpha_{df\_\text{in}} \\ 0 & \text{if} \quad R_{\text{in}} + r_b \leq \rho_i \quad \text{and} \quad \alpha_{di\_\text{in}} \leq \alpha \leq \alpha_{df\_\text{in}} \\ R_{d\_\text{in}} + r_b - \rho_i & \text{if} \quad R_{d\_\text{in}} + r_b > \rho_i \quad \text{and} \quad \alpha_{di\_\text{in}} > \alpha > \alpha_{df\_\text{in}} \\ 0 & \text{if} \quad R_{d\_\text{in}} + r_b \leq \rho_i \quad \text{and} \quad \alpha_{di\_\text{in}} > \alpha > \alpha_{df\_\text{in}} \end{cases} \tag{36}$$

FIG. 4
Model of fault at inner race.

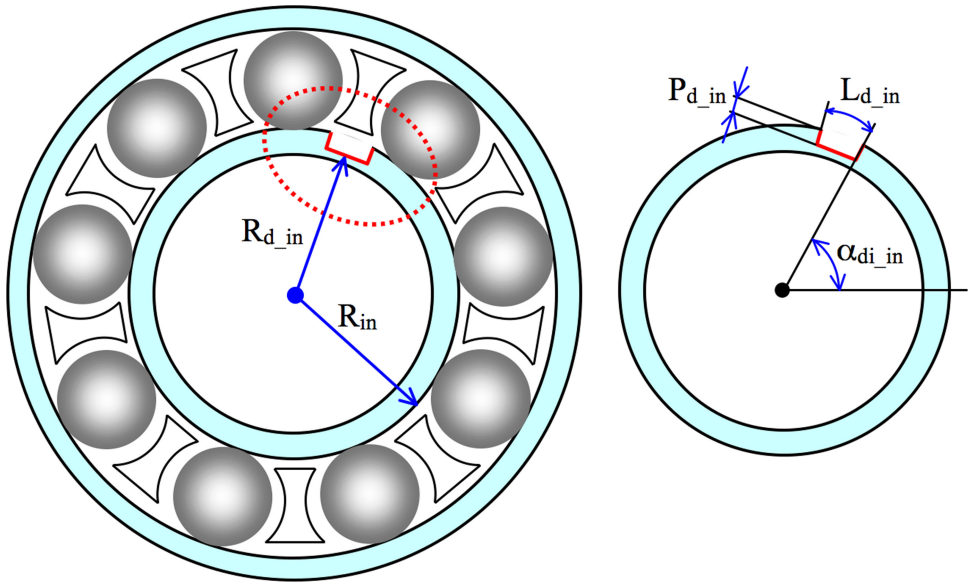

GLOBAL EQUATIONS OF THE MOVEMENT

From the previous sections, we can derive the following global equations of the movement:

- For the coordinate x_{in},

$$\sum \frac{d}{dt}\left(\frac{\partial T}{\partial \dot{x}_{in}}\right) - \sum \frac{\partial T}{\partial x_{in}} + \sum \frac{\partial U}{\partial x_{in}} + \sum \frac{\partial D_R}{\partial \dot{x}_{in}} = Q_x$$

- So, the differential equation of the movement is:

FIG. 5 Nomenclature used in fault at inner raceway.

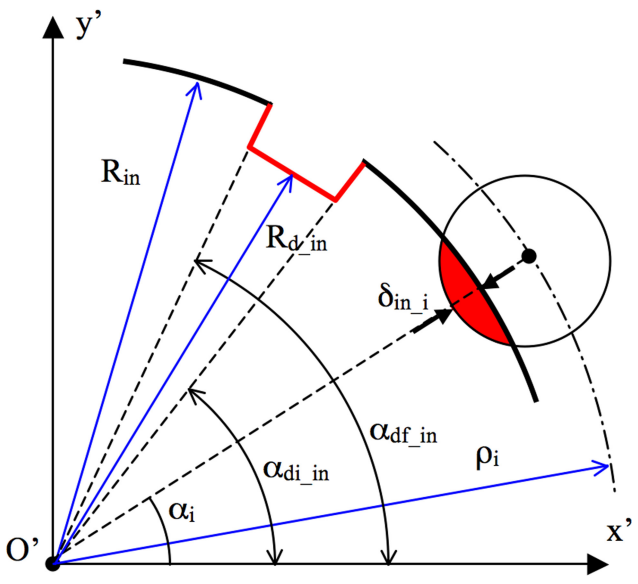

$$(m_{in} + m_{rotor})\ddot{x}_{in} - \left[\sum_{i=1}^{Z} C_{in}\delta_{in\_i}^{3/2} + D_{in}\dot{r}_i\Gamma_{in}\right]\frac{x_{in} - r_i\cos(\alpha_i)}{\rho_i} = F_{ex} + Fu\cos\alpha_{in} \quad (37)$$

- For the coordinate y_{in},

$$\sum \frac{d}{dt}\left(\frac{\partial T}{\partial \dot{y}_{in}}\right) - \sum \frac{\partial T}{\partial y_{in}} + \sum \frac{\partial U}{\partial y_{in}} + \sum \frac{\partial D_R}{\partial \dot{y}_{in}} = Q_y$$

the differential equation of the movement is:

$$(m_{in} + m_{rotor})(\ddot{y}_{in} - g) - \left[\sum_{i=1}^{Z} C_{in}\delta_{in\_i}^{3/2} + D_{in}\dot{r}_i\Gamma_{in}\right]\frac{y_{in} - r_i sin(\alpha_i)}{\rho_i} = F_{ey} + Fu\sin\alpha_{in} \quad (38)$$

- For the coordinate r_i,

$$\sum \frac{d}{dt}\left(\frac{\partial T}{\partial \dot{r}_i}\right) - \sum \frac{\partial T}{\partial r_i} + \sum \frac{\partial U}{\partial r_i} + \sum \frac{\partial D_R}{\dot{r}_i} = Q_{rj}, \quad i = 1, 2, 3, \ldots, Z$$

so, the equation of the movement is:

$$m_b\ddot{r}_i - m_b\dot{r}_i\dot{\alpha}_i^2 + m_b g\sin\alpha_i - \left[\sum_{i=1}^{Z} C_{in}\delta_{in\_i}^{3/2} + D_{in}\dot{r}_i\Gamma_{in}\right]\frac{\partial\rho_i}{\partial r_i} + C_{out}\delta_{out\_i}^{3/2} + D_{out}\dot{r}_i\Gamma_{out} = 0$$

$$\Gamma_{in} = 0 \quad \text{if} \quad \delta_{in} < 0;\ \Gamma_{in} = 1 \text{ if } \delta_{in} \geq 0$$

$$\Gamma_{out} = 0 \quad \text{if} \quad \delta_{out} < 0\ ;\ \Gamma_{out} = 1 \text{ if} \delta_{out} \geq 0 \quad (39)$$

where $i = 1, 2, 3, \ldots, Z$

Simulation Analysis

The simulation analysis carried out from the movement equations that model the behavior of the rolling element bearing is presented in this section. MATLAB and SIMULINK have been chosen as the platforms to make the different analyses because of the high capabilities that this software presents as a tool for modeling and simulating general processes. The differential equations that model the process and the movement of the elements in the bearing can be easily implemented, and also the parameters can be easily modified with the purpose of analyzing several behaviors.

MATLAB and SIMULINK have been usually employed in many systems as a modeling and simulation tool. Moreover, this simulation software has been used on several occasions as a tool to simulate certain systems or components of rolling element bearings. Thus, for example, MATLAB-based software is used to provide a framework for in-depth simulation of motor system dynamics [36]. This tool is used to process the data acquired by the system with different operating and loading conditions, in a cost-effective and time-efficient manner. MATLAB is employed in this case to process the data experimentally obtained. Finally, Liu et al. [37] uses MATLAB for monitoring the roller bearing conditions with the purpose of applying a feature-selection technique to the data obtained from vibration signals. However, MATLAB and SIMULINK have not been employed to generate the signals and movement conditions on rolling element bearings until now. In this paper we make use of these equations to generate the movement signals of each element that constitute the bearing. Once the equations are processed, different conditions can be simulated.

The parameters of the rolling element bearing are saved in a configuration file. In the simulation scheme, the movement equations obtained in the previous section are included. Also, a global reference system located in the center of the outer race (stationary) is assumed.

Table 2 represents the parameters used for the simulation of the previously modeled system. These values were obtained through the geometric analysis of the rolling bearing employed in the experimental study (as was done with the application of Hertz' theory [1]). In this work, the calculation of these parameters are not presented but the results of calculations are similar to those proposed in the literature by other authors [1]. This will enable the analysis from the simulation to be subsequently compared with experimental data obtained on the specially developed testbench. The selected data used in simulation correspond to the values of a commercial ball bearing element (SKF 6206). In this way, it will be possible to compare and validate the simulation results achieved with regard to the experimental results obtained with this real bearing.

TABLE 2 Values of the parameters used for the rolling bearing element.

Item	Value	Unit	Item	Value	Unit
ω_{in}	600–3000	rpm	r_b	4.75	mm
R_{in}	18.25	mm	R_{out}	27.75	mm
C_{in}	779180	N/mm$^{3/2}$	C_{out}	897760	N/mm$^{3/2}$
m_{in}	0.061	kg	m_{out}	0.075	kg
m_b	0.0035	kg	m_{rotor}	1.5	kg
D_{in}	0.2	N·s/mm	D_{out}	0.2	N·s/mm
F_u	0	N	F_e	0	N
h	0.01	mm	Z	3 and 9	
r_i^o	23	mm	Vr_i^o	0	m/s
Vx_{in}^o	0	m/s	Vy_{in}^o	0	m/s

SIMULINK offers multiple possibilities for carrying out a simulation via the differential equations that govern the system's behavior. The procedure of simulation employed uses the Runge-Kutta 4th–5th order method. This is a fixed-step simulation method. The period chosen is 0.1 ms. To suppress the transitory state at the beginning of the simulation, a total of 1.2 s is simulated and data relating to the initial 0.2 s is eliminated. The transitory state is thus avoided, and based on specific initial conditions, we may focus on its steady state.

It is necessary to set some conditions regarding the specific operating parameters. This will allow us to contrast the results of the simulation (obtained via equations of movement) with regard to the experimental results (obtained via the use of the developed testbed). We now list these values to be used in the simulation:

1. The initial position of the center of the inner ring (x_{in}^o, y_{in}^o) will be taken as the static deflexion experienced by the rolling bearing under load conditions.
2. The conditions of the bearing's spin velocity will be variable: 5, 10, 15, 20, 25, 30, 40, and 50 Hz (300, 600, 900, 1200, 1500, 1800, 2400, and 3000 rpm) and the radial load applied to the rolling bearing will be 3000 N. These values are usual in conventional machines.

Next, graphics are presented that show the results of $\ddot{y}_{in}$ obtained by simulation, in different conditions for models with 5 and 11 DOF (three and nine balls, respectively). To contrast these results with those obtained in the developed experimental system, which will be presented in the following section, the behavior of the rolling bearing under vibration has been simulated at different speeds.

In **Fig. 6**, we show the results of $\ddot{y}_{in}$ achieved by simulation of vibration at different speeds (5, 10, 20, 30, and 40 Hz) of models with 5 DOF (three balls). In these figures, we can see the modulated peaks that correspond to the presence of the defect in the inner ring. **Figure 7** represents envelope power spectrums, determined via the FFT (fast Fourier transform) of each of the temporal envelope of signals obtained in the simulation at each velocity. In this figure, we can observe a dominant peak very close to the ball passing inner race frequency.

FIG. 6

Signals obtained of the proposed model, which has 5 DOF for different speeds (Hz) of inner race.

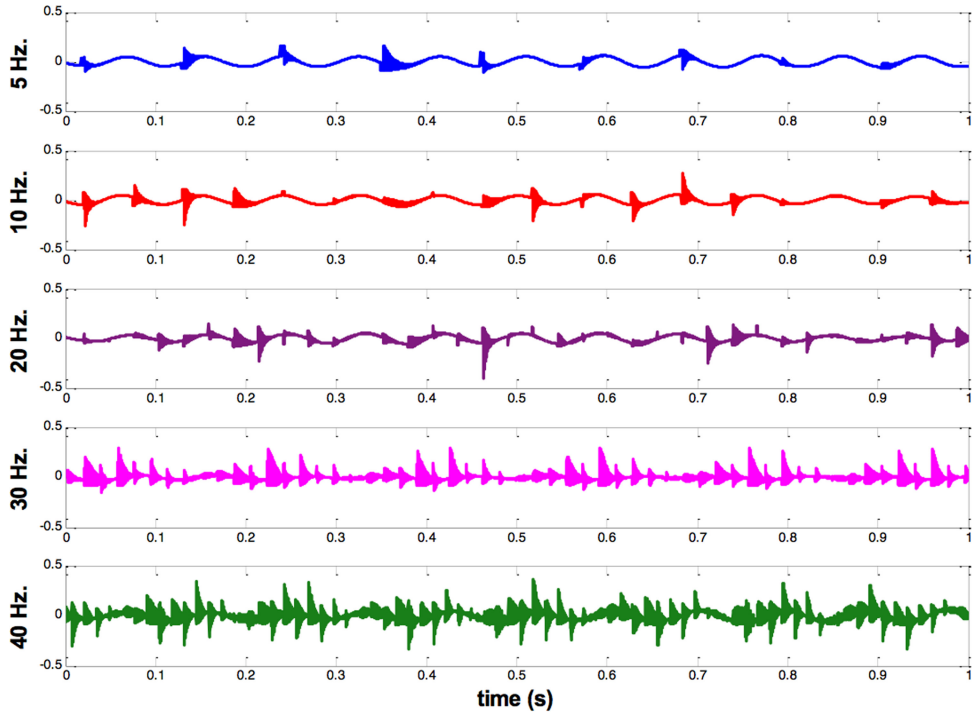

FIG. 7

Envelope power spectrum of signals shown in Fig. 6.

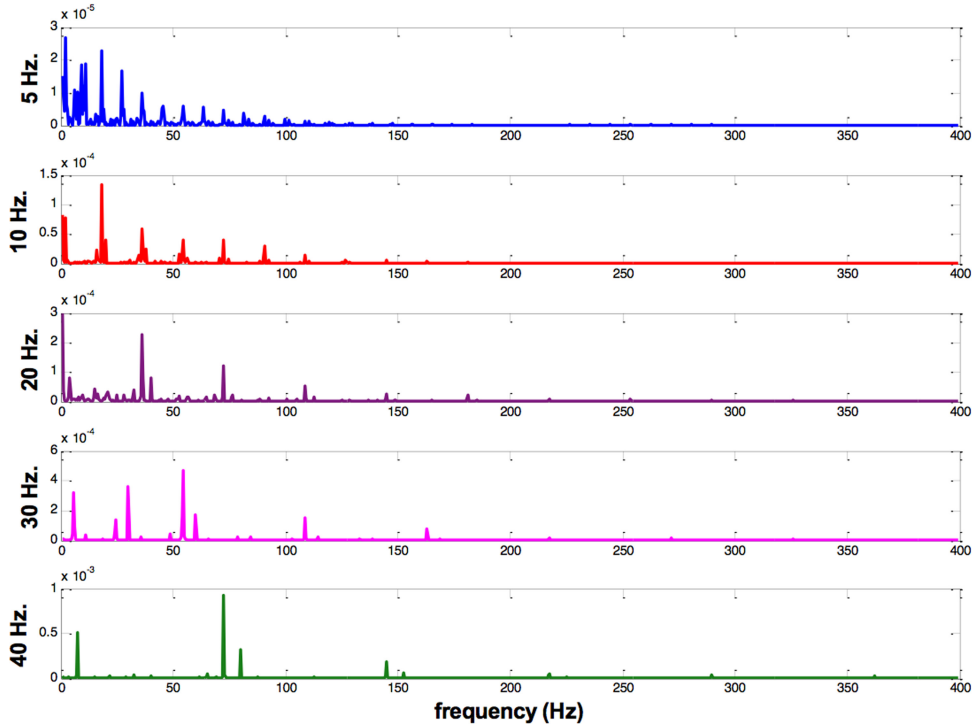

FIG. 8

Signals obtained of the proposed model, which has 11 DOF for different speeds (Hz) of inner race.

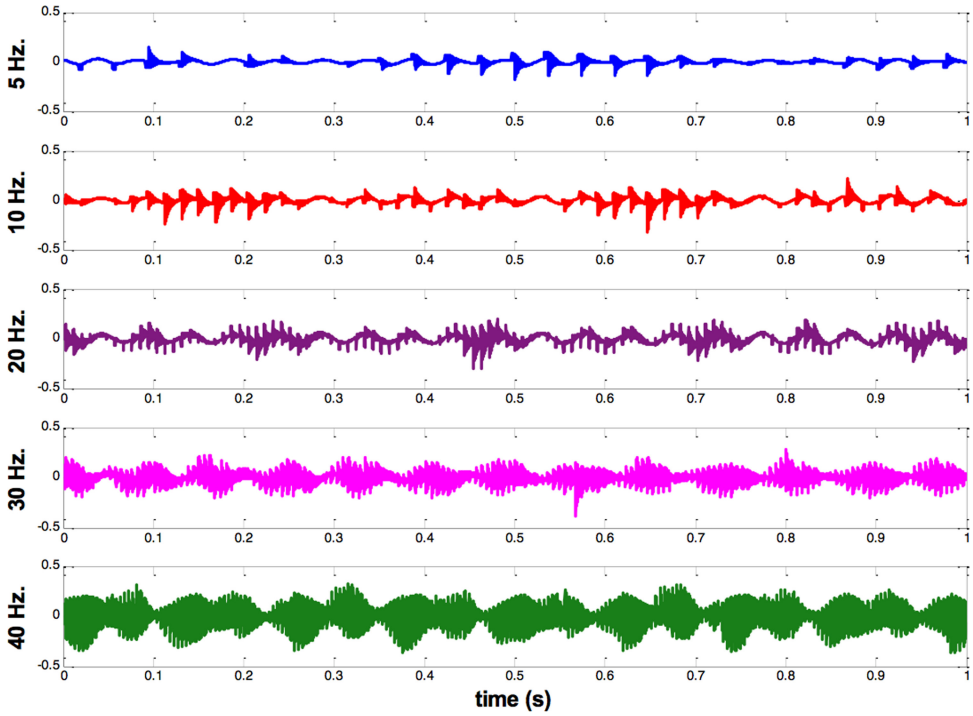

FIG. 9

Envelope power spectrum of signals shown in Fig. 8.

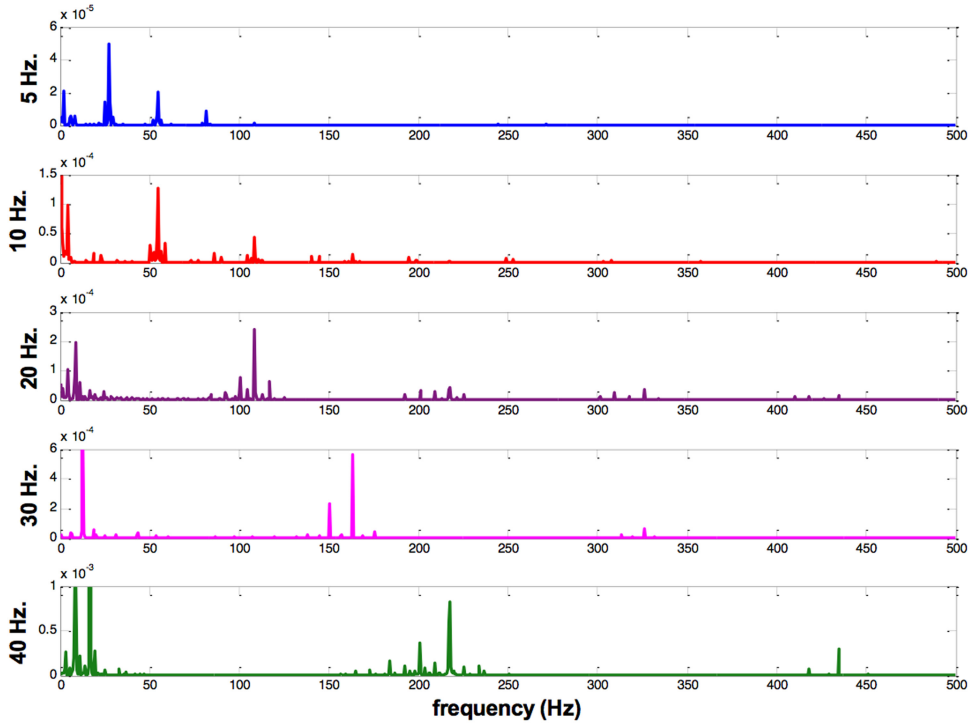

FIG. 10

(a) Testbed, and (b) rolling bearing element: I, outer race; II, inner race; III, balls; IV, cage; V, assembling tool.

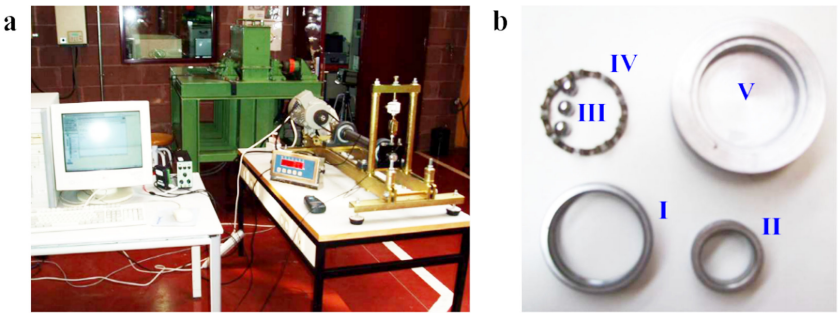

Finally, **Fig. 8** presents results of $\ddot{y}_{in}$ achieved by simulation of vibration at different speeds of model with 11 DOF (nine balls). Also we can see the modulated peaks that correspond to the presence of the defect in the inner ring. As we can observe the frequency of these peaks is bigger because of the number of balls passing through the defect. Also, **Fig. 9** represents envelope power spectrums. We observe a dominant peak very close to the ball passing inner race frequency.

Experimental Setup

With the aim of comparing the results achieved in simulation, a testbed has been developed. This testbed allows acquisition of multiple signals of mechanical vibrations from the elements of the rolling bearing when it is subject to different load conditions. The main features of this platform are the following:

1. The testbed allows reproduction of the variables analyzed and previously simulated. For this reason, the platform has a mechanism that allows application of different loads on the rolling bearing. The loads can be applied as axial or radial forces on the rolling bearing.
2. The force applied to the bearing element must to be controlled and sensed directly in a simple way. This can be accomplished through a load cell.
3. The testbed must have the ability to control properly and accurately the rotation speed, keeping the selected reference with an error less than 0.5 %.
4. The testbed must allow a simple coupling of the rolling bearing to carry out multiple tests

Taking into account these characteristics to obtain the vibration modes of the structure, the platform is developed by means of steel beams that provides high rigidity, high damping coefficients, and nominal frequencies far away from the expected defect frequencies such as misalignments, unbalance, possible faults in the rolling bearings, etc. An image of the developed testbed is shown in **Fig. 10**.

On the main structure, two rolling bearings are added. These rolling bearings support the main shaft. This shaft, in its rotation movement, makes the rotation of the tested rolling bearing that is located on one side of the shaft. A fixation system composed of a washer and hexagonal bolt avoids sliding of the inner race of the tested rolling bearing over the surface of the axis. The motion from the electric motor to the main shaft is carried out through a belt. The load acting over the rolling bearing is transmitted by means of two spindles working axially and radially. The control of the load acting over the rolling bearing is performed by means of two load cells. These load cells have a range under 10 000 N. The roller bearing housing has been designed with the purpose of providing an easy system to change the bearing without the necessity of using special tools.

We have designed this part paying particular attention to the working frequencies of vibration. The purpose is that these frequencies were further away than the expected vibration frequencies generated in rolling bearings with a fault. The speed

FIG. 11

Rolling bearing of (a) nine balls, and (b) three balls.

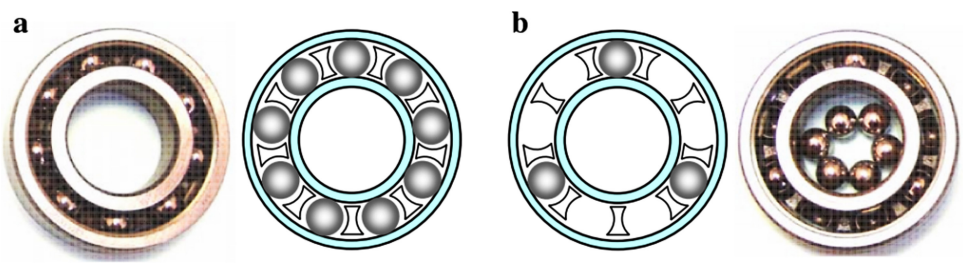

FIG. 12

Experimental signal for inner race detect.

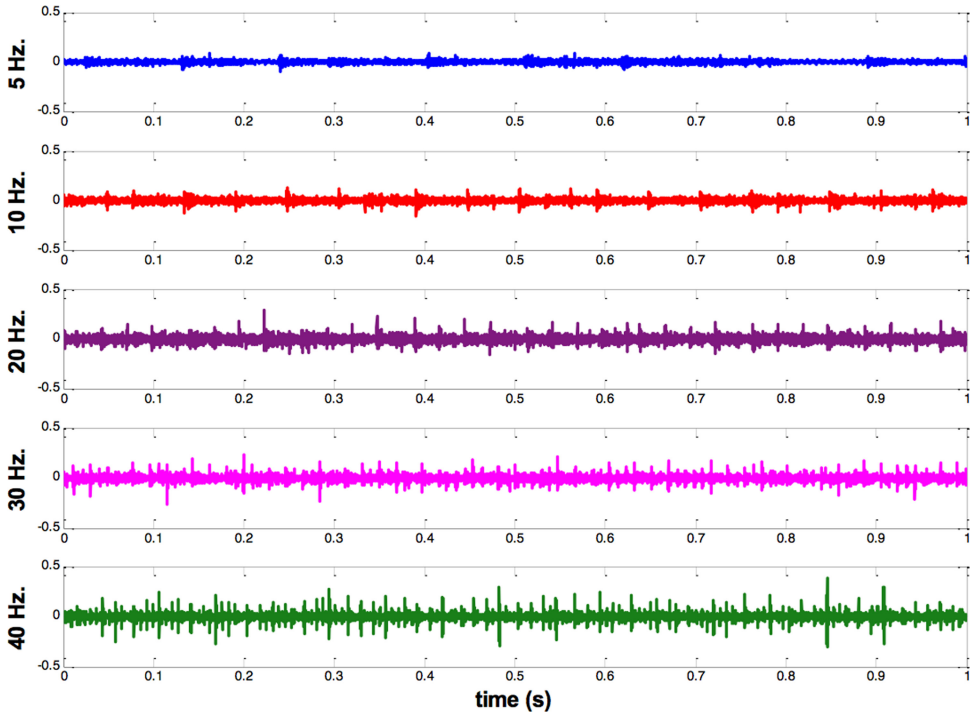

FIG. 13

Envelope power spectrum of signals shown in Fig. 12.

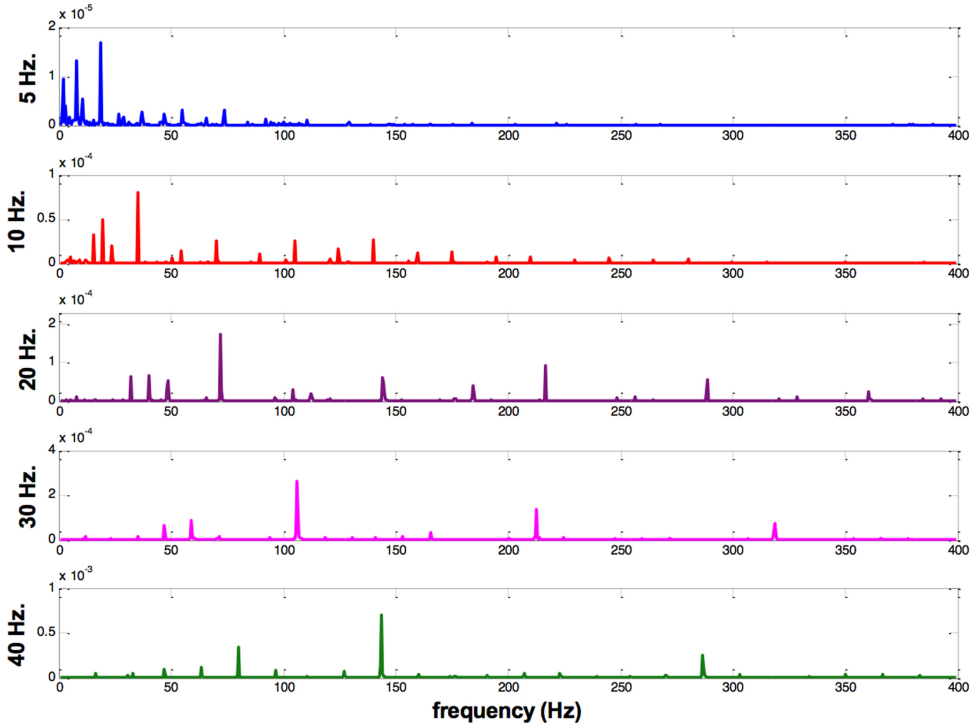

FIG. 14 (a) Experimental signal ($\ddot{y}_{in}$), and (b) signal obtained from the proposed model with 5 DOF.

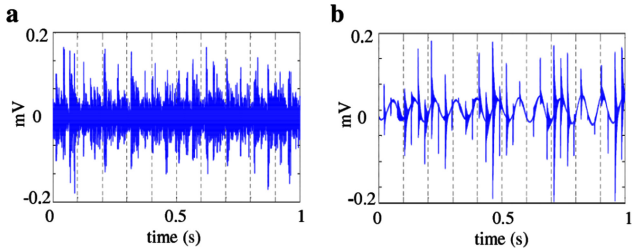

control of the electric motor is accomplished by means of a frequency inverter. The frequency of the output currency can be modified from 0 to 110 Hz allowing a variation in the speed of the motor beyond 3000 rpm.

For the experimental analysis of the system with 5 DOF (three balls), as the commercial ball bearing had nine balls, six were extracted, leaving a ball bearing with three evenly spaced balls.

To get a representative experimental signal for each case studied, and to minimize any randomness associated with experiments, a large number of tests have been carried out as follows. The experiment is composed of 10 trials. For each test, we employed 10 different bearings. For each of these bearings, 10 data files were extracted (samples acquired at different time intervals). So the result of each experiment (shown in the figures) is composed by 1000 measures. In these experiments we have employed:

- New ball bearings and rolling bearings with localized defects.
- Bearings of nine and three balls (**Fig. 11**).
- The speed has been varied through 5, 10, 15, 20, 25, 30, 40, and 50 Hz.

Figures 12 and **13**, represent one example of the experimental results of $\ddot{y}_{in}$ obtained for the system with 5 DOF (three balls) when the ball bearing is submitted to different speeds. The tests were carried out at the same velocities as those done under simulation with the aim of contrasting the results. **Figure 12** shows the data obtained in one of these tests under different speeds (5, 10, 20, 30, and 40 Hz). This result corresponds to a test of a rolling bearing with three balls and with one localized defect in its inner ring. Also, **Fig. 13** shows the fast Fourier transform of these temporal envelope of signals.

Overall Analysis

In this section, we compare the signals obtained in simulation with the result obtained with real equipment. To compare these signals we have employed the fast Fourier transform of both signals achieving the envelope power spectrum.

Figure 14(*a*) and **14(*b*)** show, for a bearing with an inner race localized defect, the experimental signal and the simulated

FIG. 15 Envelope power spectrum of signals shown in Fig. 14.

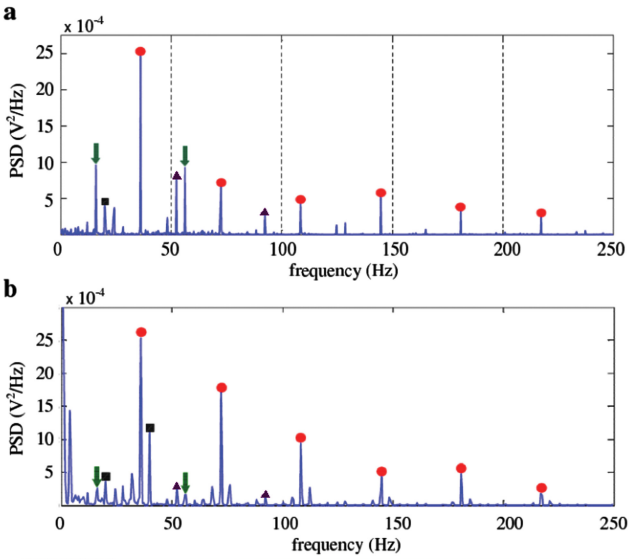

signal, respectively. Also, the frequency spectrum of the signal and those obtained from the acceleration response of the proposed model are shown in **Fig. 15(*a*)** and **15(*b*)**, respectively.

As we can see in **Fig. 15(*a*)**, the envelope power spectrum contains a dominant peak very close to the ball passing the inner race frequency (36.2 Hz). The peaks that ended with point are the harmonic of defect frequency. This figure shows also a peak at 20 Hz (ended with a square) corresponding to the rotation frequency. **Figure 15(*b*)** is the envelope power spectrum of the acceleration response obtained from the proposed model. As it can be seen, there is a dominant peak at 36.19 Hz, which is almost near to the ball passing inner race frequency. Harmonics also appear at the frequency of the defect (peaks ended with point) and peak of the rotation frequency (ended with square). The peak that ended with an arrow (16.2 Hz–56.2 Hz) and the peak that ended with a triangle (52.4 Hz–92.0 Hz) are sidebands of the first and second harmonic of the fault frequency, respectively. The above study shows that the main contributions of the envelope power spectrum obtained by the proposed model are in accordance with the reported experimental spectra for an inner race defect condition.

With the purpose of comparing the large set of results in the tests and the corresponding simulations, we have analyzed the time evolutions of the spectral power. **Figure 16** shows the experimental data and the simulations of the models to compare them. We can see the evolution graphs of spectral power concerning the speed of the inner race, for the bearing of 5 DOF (**Fig. 16(*a*)**) and for the bearing of 11 DOF (**Fig. 16(*b*)**), both without defect. Also, in this figure, we show the same simulations and the experimental results with a defect in the inner race for the bearing of 5 DOF (**Fig. 16(*c*)**) and for the bearing of

FIG. 16

Spectral power evolution of signal as in experimental (squares) and as in simulated (circles) data.

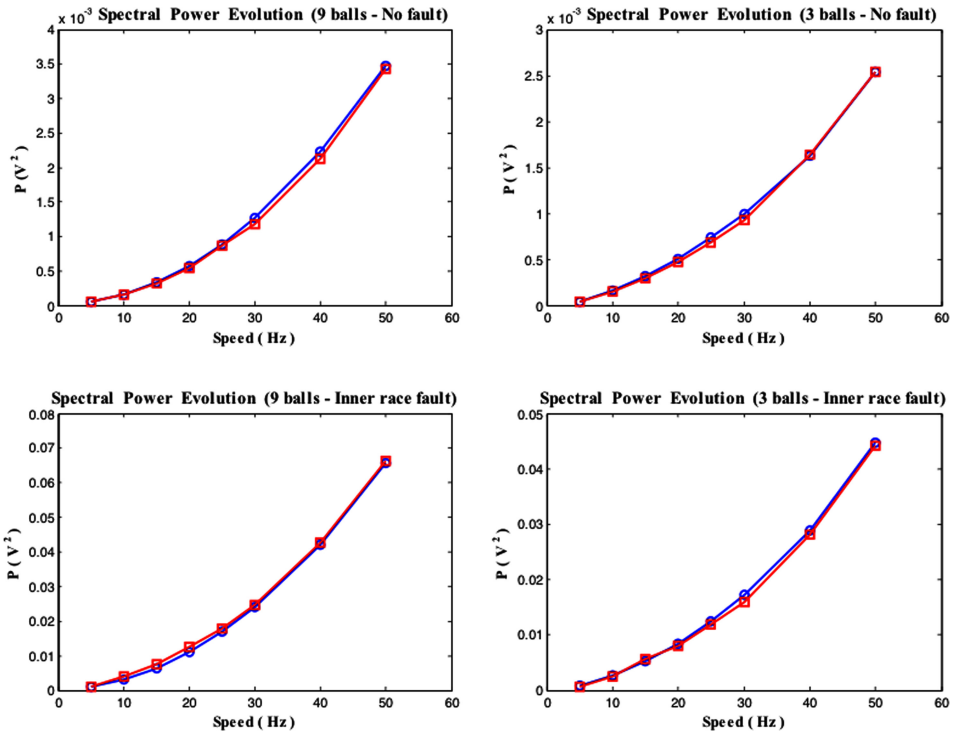

11 DOF (**Fig. 16(*d*)**). The experimental values are according to the average of the test results.

It is observed that in all cases the obtained simulation results match with the experimental results. This is true for rolling bearings without defect and rolling bearings containing localized surface defects on the inner raceway. We also observe the same trend in each case as speed increases. As we can deduce from the figures, the value of the spectral power in the case of a rolling bearing without defect is lower than the defective rolling bearing.

Conclusions

A new analytic model of dynamic behavior of a ball bearing with or without localized defects has been presented by applying Lagrange's formulation. The integration of non-linear equations of motion were carried out on MATLAB by using the Runge Kutta 4th–5th order method.

The ball bearing model allows for the possibility of varying geometric, kinematic, structural (stiffness and damping in contact), or dynamic parameters, as well as the presence of localized defects in its inner or outer ring. By means of the simulation of the model we can estimate the radial position, velocity, and acceleration of the balls in the bearing and the central point of the inner ring, forces, and shifts in the contacts, etc.

The model has been tested for a configuration of three balls (5 DOF) and nine balls (11 DOF) to better appreciate the phenomena associated with its operation and was also tested for the operating conditions of a conventional machine. The simulation results obtained using the analytical model (vibrations) agree reasonably well with the predictions. A well-defined temporary signal was obtained along with various spectrums where the dominant harmonics are usually associated with the FFT of the ball bearing. The presence of defects in the model originates dominant peaks in the frequency of the defect.

The vibratory behavior of the analytic ball bearing model has been experimentally compared by means of a testbed specifically designed to sense these characteristics. We have presented simulation results of several ball bearings that have been employed in real experiments in the testbed. When comparing results obtained from the dynamic bearing model with the experimental results, using the evolution of the spectral power, we can observe a similar behavior. Thus, we can conclude that the analytical model presented has been validated through experimental results in real cases.

References

[1] Harris, T. A., *Rolling Bearing Analysis*, 4th ed., Wiley, Hoboken, NJ, 2001.

[2] Changsen, W., *Analysis of Rolling Element Bearings*, Mechanical Engineering, London, 1991.

[3] Wang, H. and Chen, P., "Fault Diagnosis for a Rolling Bearing Used in a Reciprocating Machine by Adaptive Filtering Technique and Fuzzy Neural Networks," *WSEAS Trans. Syst.*, Vol. 7, No. 1, 2008, pp. 1–6. Available at http://www.wseas.us/e-library/transactions/systems/2008/2007-526N.pdf

[4] Cao, Y. and Altintas, Y., "A General Method for the Modeling of Spindle-Bearing Systems," *J. Mech. Design*, Vol. 126, 2004, pp. 1089–1104.
[5] Walters, C. T., "The Dynamics of Ball Bearings," *J. Lubr. Eng.*, Vol. 93, 1971, pp. 1–10.
[6] Wensing, J., 1998, "On the Dynamics of Ball Bearings," Ph.D. thesis, University of Twente, The Netherlands.
[7] Dietl, P., Wensing, J., and van Nijen, G., "Rolling Bearing Damping for Dynamic Analysis of Multi-Body Systems—Experimental and Theoretical Results," *J. Multi-Body Dyn.*, Vol. 214, No. 1, 2000, pp. 33–43.
[8] Sarangi, M., Majumdar, B. C., and Sekhar, A. S., "On the Dynamics of Elastohydrodynamic Mixed Lubricated Ball Bearings. Parts I and II," *J. Eng. Tribol.*, Vol. 219, 2005, pp. 411–433.
[9] Gupta, P. K., *Advanced Dynamics of Rolling Element Bearings*, Springer Verlag, Berlin, 1984.
[10] Gupta, T. C., Gupta, K., and Sehgal, D. K., "Nonlinear Vibration Analysis of an Unbalanced Flexible Rotor Supported by Ball Bearings With Radial Internal Clearance," *Proceedings of the 53rd ASME Turbo Expo 2008*, Vol. 5, Part A, Berlin, Germany, June 9–13, 2008, pp. 1289–1298.
[11] Tiwari, M., Gupta, K., and Prakash, O., "Experimental Study of a Rotor Supported by Deep Groove Ball Bearing," *Int. J. Rotat. Mach.*, Vol. 8, No. 4, 2002, pp. 243–258.
[12] Kennel, J. W. and Bupara, S. S., "A Simplified Model of Cage Motion in Angular Contact Bearings Operating in the EHD Lubricating Regime," *J. Lubr. Technol.*, 1978, Vol. 101, pp. 395–401.
[13] Meeks, C., "Ball Bearing Dynamic Analysis Using Computer Methods and Correlation With Empirical Data," *International Tribology Conference*, Melbourne, Australia, Dec 2–4, 1987.
[14] Fukata, S., Gad, E., Kondou, T., Ayabe, T., and Tamura, H., "On the Radial Vibrations of Ball Bearings (Computer Simulation)," *Bull. JSME*, Vol. 44, 1985, pp. 83–111.
[15] Meeks, C. and Tran, L., "Ball Bearing Dynamic Analysis Using Computer Methods. Part I Analysis," *J. Tribol.*, Vol. 118, 1996, pp. 52–58.
[16] Harsha, S. P., "Non-Linear Dynamic Response of a Balanced Rotor Supported on Rolling Element Bearings," *Mech. Syst. Signal Proc.*, Vol. 19, 2005, pp. 551–578.
[17] Harsha, S. P., "Nonlinear Dynamic Analysis of a High-Speed Rotor Supported by Rolling Element Bearings," *J. Sound Vib.*, Vol. 290, 2006, pp. 65–100.
[18] Harsha, S. P., Sandeep, K., and Prakash, R., "Effects of Preload and Number of Balls on Nonlinear Dynamic Behaviors of Ball Bearing System," *Int. J. Nonlin. Sci. Numer. Sim.*, Vol. 4, No. 3, 2003, pp. 265–278.
[19] Nataraj, C. and Harsha, S. P., "The Effect of Bearing Cage Run-Out on the Nonlinear Dynamics of a Rotating Shaft," *Commun. Nonlin. Sci. Numer. Sim.*, Vol. 13, 2008, pp. 822–838.
[20] Upadhyay, S. H., Harsha, S. P., and Jain, S. C., "Analysis of Nonlinear Phenomena in High Speed Ball Bearings due to Radial Clearance and Unbalanced Rotor Effects," *J. Vib. Control*, Vol. 16, No. 1, 2010, pp. 65–88.
[21] Purohit, R. K., "Dynamic Analysis of Ball Bearings With Effect of Preload and Number of Balls," *Int. J. Appl. Mech. Eng.*, Vol. 11, No. 1, 2006, pp. 77–91. Available at http://www.ijame.uz.zgora.pl/ijame_files/archives/v11PDF/n1/77-91_Article_05.pdf
[22] Feng, N., Hahn, E., and Randall, R., "Simulation of Vibration from a Rolling Element Bearing Defect," *International Conference on Health and Usage Monitoring*, Melbourne, Australia, Feb 19–20, 2001, pp. 37–52.
[23] Bhattacharyya, K. and Mukherjee, A., "Modeling and Simulation of Centerless Grinding of Ball Bearings," *Sim. Modell. Pract. Theory*, Vol. 14, 2006, pp. 971–988.
[24] Klang, Y., Shen P., Huang, Ch., Shyr, S., and Chang, Y., "A Modification of the Jones-Harris Method for Deep-Groove Ball Bearings," *Tribol. Int.*, Vol. 39, 2006, pp. 1413–1420.
[25] Rubio, H., Garcia-Prada, J. C., and Laniado, E., "Dynamic Analysis of Rolling Bearing System Using Lagrangian Model vs. Fem Code," *Proceedings of the 12th IFToMM World Congress*, Besançon, France, June 18–21, 2007.
[26] Chen, M., Meng, G., and Wu, B., "Nonlinear Dynamics of a Rotor-Ball Bearing System With Alford Force," *J. Vib. Control*, Vol. 18, No. 1, 2012, pp. 17–27.
[27] Dougdag, M., Ouali, M., Boucherit, H., Titouche, N. E., and Djaoui, M., "An Experimental Testing of a Simplified Model of a Ball Bearing: Stiffness Calculation and Defect Simulation," *Meccanica*, Vol. 47, 2012, pp. 335–354.
[28] Gao, X. H., Huang, X. D., Wang, H., and Chen, J., "Modelling of Ball-Raceway Contacts in a Slewing Bearing With Non-Linear Springs. Proceedings of the Institution of Mechanical Engineers, Part C," *J. Mech. Eng. Sci.*, Vol. 225, No. 4, 2011, pp. 827–831.
[29] Kappaganthu, K. and Nataraj, C., "Nonlinear Modeling and Analysis of a Rolling Element Bearing With a Clearance," *Commun. Nonlin. Sci. Numer. Simul.*, Vol. 16, 2011, pp. 4134–4145.
[30] Slavič, J., Brković, A., and Boltežar, M., "Typical Bearing-Fault Rating Using Force Measurements: Application to Real Data," *J. Vib. Control*, Vol. 17, No. 14, 2011, pp. 2164–2174.
[31] Tadina, M. and Boltezar, M., "Improved Model of a Ball Bearing for the Simulation of Vibration Signals because of Faults during Run-Up," *J. Sound Vib.*, Vol. 330, 2011, pp. 4287–4301.
[32] Ahmad, R., Saeed, A., Anoushiravan, F., and Hamid, M., "Nonlinear Dynamic Modeling of Surface Defects in Rolling Element Bearing Systems," *J. Sound Vib.*, Vol. 319, 2009, pp. 1150–1174.
[33] SIMULINK; *Dynamic Simulation for* MATLAB. (1999). The Math Works, Natick, MA.
[34] Braut, S., Zigulić, R., and Butković, M., "Numerical and Experimental Analysis of a Shaft Bow Influence on a Rotor to Stator Contact Dynamics," *J. Mech. Eng.*, Vol. 54, No. 10, 2008, pp. 693–706. Available at http://cat.inist.fr/?aModele=afficheN&cpsidt=20807799
[35] Bai, C. Q., Zhang, H. Y., and Xu, Q. Y., "Effects of Axial Preload of Ball Bearing on the Nonlinear Dynamic Characteristics of a Rotor-Bearing System," *Nonlinear Dynam.*, Vol. 53, No. 3, 2008, pp. 173–190.
[36] Li, B., Chow, M., Tipsuwan, Y., and Hung, J. C., "Neural-Network-Based Motor Rolling Bearing Fault Diagnosis," *IEEE Trans. Ind. Electron.*, Vol. 47, No. 5, 2000, pp. 1060–1069.
[37] Liu, T., Ordukhani, F., and Jani, D., "Monitoring and Diagnosis of Roller Bearing Conditions Using Neural Networks and Soft Computing," *Int. J. Knowl.-Based Intell. Eng. Syst.*, Vol. 9, No. 2, 2005, pp. 149–157.